

# Spark plasma sintering as an effective texturing tool for reprocessing recycled HDDR Nd-Fe-B magnets with lossless coercivity

Ikram, Awais; Awais, Muhammad; Sheridan, Richard; Walton, Allan; Kobe, Spomenka; Pušavec, Franci; Rozman, Kristina Zuzek

DOI:  
[10.3390/met10030418](https://doi.org/10.3390/met10030418)

License:  
Creative Commons: Attribution (CC BY)

*Document Version*  
Publisher's PDF, also known as Version of record

*Citation for published version (Harvard):*  
Ikram, A, Awais, M, Sheridan, R, Walton, A, Kobe, S, Pušavec, F & Rozman, KZ 2020, 'Spark plasma sintering as an effective texturing tool for reprocessing recycled HDDR Nd-Fe-B magnets with lossless coercivity', *Metals*, vol. 10, no. 3, 418, pp. 1-17. <https://doi.org/10.3390/met10030418>

[Link to publication on Research at Birmingham portal](#)

## General rights

Unless a licence is specified above, all rights (including copyright and moral rights) in this document are retained by the authors and/or the copyright holders. The express permission of the copyright holder must be obtained for any use of this material other than for purposes permitted by law.

- Users may freely distribute the URL that is used to identify this publication.
- Users may download and/or print one copy of the publication from the University of Birmingham research portal for the purpose of private study or non-commercial research.
- User may use extracts from the document in line with the concept of 'fair dealing' under the Copyright, Designs and Patents Act 1988 (?)
- Users may not further distribute the material nor use it for the purposes of commercial gain.

Where a licence is displayed above, please note the terms and conditions of the licence govern your use of this document.

When citing, please reference the published version.




## Take down policy

While the University of Birmingham exercises care and attention in making items available there are rare occasions when an item has been uploaded in error or has been deemed to be commercially or otherwise sensitive.

If you believe that this is the case for this document, please contact [UBIRA@lists.bham.ac.uk](mailto:UBIRA@lists.bham.ac.uk) providing details and we will remove access to the work immediately and investigate.

## Article

# Spark Plasma Sintering as an Effective Texturing Tool for Reprocessing Recycled HDDR Nd-Fe-B Magnets with Lossless Coercivity

Awais Ikram <sup>1,2,3,\*</sup> , Muhammad Awais <sup>4</sup> , Richard Sheridan <sup>4</sup>, Allan Walton <sup>4</sup>, Spomenka Kobe <sup>2,3</sup> , Franci Pušavec <sup>1</sup> and Kristina Žužek Rožman <sup>2,3</sup>

<sup>1</sup> Faculty of Mechanical Engineering, University of Ljubljana, Aškerčeva cesta 6, SI-1000 Ljubljana, Slovenia; franci.pusavec@fs.uni-lj.si

<sup>2</sup> Department for Nanostructured Materials, Jožef Stefan Institute, Jamova 39, SI-1000 Ljubljana, Slovenia; spomenka.kobe@ijs.si (S.K.); tina.zuzek@ijs.si (K.Ž.R.)

<sup>3</sup> Jožef Stefan International Postgraduate School, Jamova 39, SI-1000 Ljubljana, Slovenia

<sup>4</sup> School of Metallurgy and Materials, University of Birmingham, Edgbaston, Birmingham B15 2TT, UK; m.awais@bham.ac.uk (M.A.); r.s.sheridan.1@bham.ac.uk (R.S.); a.walton@bham.ac.uk (A.W.)

\* Correspondence: rana.awaisikram@yahoo.com; Tel.: +386-68-67-3099

Received: 23 December 2019; Accepted: 23 March 2020; Published: 24 March 2020



**Abstract:** The low-pressure hot-deformation methodology was applied to reprocess the nanocrystalline hydrogenation–disproportionation–desorption–recombination (HDDR) Nd-Fe-B powders from end-of-life (EOL) permanent magnets’ waste to determine the mechanism of texture development and the resultant improvement in remanence (and  $BH_{max}$ ) in the recycled material. Both the hot-pressed and hot-deformed magnets produced via spark plasma sintering (SPS) were compared in terms of their magnetic properties with respect to forging pressures. Also, a comparison was established with the microstructure to cite the effectiveness of texture development at low deformation rates and pressures which is pivotal for retaining high coercivity. The hot-pressed magnets maintain the high coercivity (better than 100%) of the original recycled powder due to the control of SPS conditions. The hot deformation pressure was varied from 100–150 MPa at 750 °C processing temperature to identify the optimal texture development in the sintered HDDR Nd-Fe-B magnets. The effect of post-hot-deformation thermal treatment was also investigated, which helped in boosting the overall magnetic properties and better than the recycled feedstock. This low-pressure hot deformation process improved the remanence of the hot-pressed magnet by 11% over the starting recycled powder. The  $M_r/M_s$  ratio which was 0.5 for the hot-pressed magnets increased to 0.64 for the magnets hot-deformed at 150 MPa. Also, a 55% reduction in height of the sample was achieved with the c-axis texture, indicating approximately 23% higher remanence over the isotropic hot-pressed magnets. After hot deformation, the intrinsic coercivity ( $H_{Ci}$ ) of 960 kA/m and the remanence ( $B_r$ ) value of 1.01 T at 150 MPa is indicative that the controlled SPS reprocessing technique can prevent microstructure related losses in the magnetic properties of the recycled materials. This route also suggests that the scrap Nd-Fe-B magnets can be treated with recoverable magnetic properties subsequently via HDDR technique and controlled hot deformation with a follow-up annealing.

**Keywords:** rare earth permanent magnets; anisotropic HDDR Nd<sub>2</sub>Fe<sub>14</sub>B; recycling; spark plasma sintering; texture development; hot deformation

## 1. Introduction

The rare-earth based Nd-Fe-B permanent magnets (REPMs) are vital components for modern electronics, energy, medical imaging, and automotive industries due to their high magnetization and magnetostatic energy confined in a small volume ( $BH_{max}$ ). These excellent magnetic properties

ascend from a combination  $4f$  rare earth (RE) sublattices contributing to high magnetocrystalline anisotropy and  $3d$  transition metal (TM) sublattices return high magnetization, energy product and Curie temperature [1]. The  $BH_{max}$  is approximated to value  $J_r^2/4\mu_0$  ( $J_r$  is the remnant polarization and related to magnetic induction as:  $J = B - \mu_0 H$ , such that  $\mu_0$  is the permeability of free space), in the case when the coercivity ( $H_{Ci}$ -resistance to demagnetization) is nominally  $\frac{1}{2} J_r$  [2]. Nanocrystalline Nd-Fe-B alloys are developed to retain the high coercivity in bulk magnets by virtue of their ultrafine near single-domain sized grains. Coercivity will be very high as the reverse domains in a magnetically decoupled system will not spread easily and their movement at low external demagnetizing fields can be reduced by the pinning sites. Moreover, the probability of defects is lower in these smaller near single domain sized grains [3,4]. Nanocrystalline Nd-Fe-B alloys cannot be conventionally sintered which eludes their high coercivity exploitation because the ultrafine grain structure will undergo excessive grain coarsening at elevated sintering temperatures, resulting into coercivity losses. Due to this reason, either the bonded magnets are their primary application [5] or the rapid processing methodologies are applied, e.g., spark plasma sintering, hot deformation, and die-upsetting [1,6,7]. Previously we have demonstrated the control in SPS parameters resulted in high coercivity ( $H_{Ci} \approx 1200$  kA/m) of the recycled HDDR Nd-Fe-B-type isotropic magnets [7] and that the particle size has a critical significance on the sinterability and oxygen uptake of the recycled powder [8]. These microstructure-magnetic properties relationships were derived only for the isotropic magnets ( $M_r/M_s \leq 0.5$ ) processed by SPS, whereas the starting recycled HDDR Nd-Fe-B powder contains anisotropic powder particles. In order to enhance the remanence and the energy product, the hot deformation methodology is necessary [9] but unlike so far, the hot forging technique has not been adopted for the recycled HDDR Nd-Fe-B system. Besides oxygen content also plays an important role in the magnet reprocessing by hot deformation and since the recycled materials contain approximately two folds or higher oxygen content than the commercial grade materials, the processing route needs to be validated [8].

The deformation techniques produce a high degree of texture in the nanocrystalline Nd-Fe-B systems (melt-spun ribbons or hydrogenation–disproportionation–desorption–recombination (HDDR), making the anisotropic grains oriented towards the easy-axis of magnetization. To alter the direction of magnetization vector away from easy c-axis, a significantly larger external field is necessary in anisotropic magnets, such that the energy stored in the crystallites to work against the anisotropy increases as the elastic modulus becomes smaller in parallel direction to c-axis with more texture induced at high temperature pressure conditions [10]. The changes to the grain shape and aspect ratio alter the shape anisotropy, as the extent of magnetization due to an external field for a perfectly spherical ferromagnetic particle would be the same in any direction. However, for the non-spherical grains, the magnetization is easier in the longer direction (of higher aspect ratio) than the shorter axis. [4]. The high anisotropy is accredited mutually to the rotation and the preferred growth of  $Nd_2Fe_{14}B$  grains under pressure at elevated temperatures. Güth et al. [11] studied the anisotropy profiles of HDDR powder particles and suggested that the system demonstrated a biaxial {001} (100) local texture (pre-dominant crystal field interactions along the c-axis [001] i.e., the easy-axis alignment and the original grains are confined along a-axis grains). This theory was later confirmed by EBSD pole figures analysis by Sepehri-Amin et al. [12] and Kim et al. [13].

In rare-earth lean systems, the stress induced crystallographic orientation of the nanocrystalline Nd-Fe-B powders by hot deformation becomes critically difficult to achieve [14]. Early work of hot deformation by Müller et al. [15] on the isotropic HDDR Nd-Fe-B powder resulted in  $B_r = 1.1$  T and  $H_{Ci} \approx 710$  kA/m. Similarly, Kirchner et al. [16] studied the effect of Nd addition during the hot deformation and reported for 14 at.% Nd in the HDDR powder, the remanence of 1.2 T and coercivity 550 kA/m can be achieved but sample cracking was still obvious after forging. Increasing the Nd content to 16 at.% prevented the HDDR samples from cracking and improved the coercivity to 750 kA/m but the  $B_r$  reduced slightly to 1 T with the higher rare-earth content. Concurrently Gopalan et al. [17] were able to increase the remanence after hot deformation from 1.07 T to 1.35 T in the precursor HDDR powder of composition  $Nd_{14.1}Fe_{78.2}Co_{1.0}B_{6.1}Cu_{0.1}Al_{0.5}$ . Likewise, Li et al. [18] obtained  $B_r = 1.09$  T

and  $BH_{max} = 114 \text{ kJ/m}^3$  after HDDR powder hot deformation through SPS, but the  $H_{Ci}$  was only 384 kA/m, due to grain shape factor and interlinked with the abnormal grain growth of  $\text{Nd}_2\text{Fe}_{14}\text{B}$  crystallites. The hot deformation temperatures were identified by Li et al. [19], achieving 69% height reduction,  $B_r = 1.22 \text{ T}$  and yet again low  $H_{Ci} = 181 \text{ kA/m}$  and  $BH_{max} = 121 \text{ kJ/m}^3$  only. This inferior coercivity in hot-deformed HDDR Nd-Fe-B magnets tends to significantly reduce the squareness of hysteresis and lowers the  $BH_{max}$  values, even after high deformation ratio; effectively rendering such magnets unsuitable for commercial applications [9,19]. Concurrently no previous report cited the hot deformation-based reprocessing of the recycled Nd-Fe-B alloys to the extent of our literature review, but the strategic task is to revitalize the recycled powders to novel magnets, retaining loop squareness, initially by gaining high  $H_{Ci}$ , and then by tackling  $B_r$  and  $BH_{max}$ .

Evidently, the hot deformation in the HDDR Nd-Fe-B system has yielded nominal improvement in texture but at the expense of coercivity. Previously, the strain rate and the degree of deformation have been considered as the controlling factors for texture development, without quantifying the terminal pressures [9]. So, in such cases, the control on resultant squareness of hysteresis loop is lost and coercivity decline is most certain [19]. The enhancement of coercivity along with  $B_r$  in hot-deformed magnets is becoming a subject of interest due to successful application of grain boundary (GB) modification of the hot deformed melt-spun ribbons yielded high  $B_r \approx 1.4 \text{ T}$  and  $H_{Ci} > 2000 \text{ kA/m}$  [20–32]. Similarly, in case of the fresh Nd-Fe-B HDDR system, Song et al. [33] utilized Pr-Cu low melting alloys to improve the coercivity of the hot-deformed HDDR Nd-Fe-B-type magnets to 1230 kA/m. Similarly, with the addition of up to 2 wt.% Nd-Cu alloys were reported to improve the coercivity of hot-deformed magnets to 1042 kA/m [34]. A significant improvement of 640 kA/m was also indicated after the grain boundary modification treatment of the HDDR-based Nd-Fe-B magnets with milled powder blend of  $\text{NdH}_x + \text{Cu}$  [35].

However, the primary argument in view of magnetic scrap reprocessing questioned the suitability of applying hot deformation techniques to the recycled HDDR Nd-Fe-B isotropic magnets. The existing literature on the commercial grade MF15P or high performance anisotropic HDDR Nd-Fe-B powders indicated a loss in coercivity and  $BH_{max}$  after texturing/forging and possible recovery attained only with the additional grain boundary modification treatments [9,19]. Thus, we imply this requirement in the recycled material, that retention of the coercivity and the squareness of the hysteresis loop is sustained as the texture is introduced. The experimental reported work in this manuscript is an effort to validate the relationship of texturing in the microstructure with the dependent properties to match commercial counterpart magnets.

This study answers these two queries: (a) can the recycled HDDR powder (with  $\approx 4800 \text{ ppm}$  oxygen content) be forged at lower pressures in view of the reduced total rare earth (TRE) content (below 30 wt.%) [7] and (b) if the process can be controlled to obtain the magnetic properties comparable to the precursor recycled powder (with the mechanism of texturing justified with the microstructure). Low forging pressures are suitable to retain texturing process control and the degree of deformation in order to retain the squareness of hysteresis loop and lossless coercivity. The SPS system and forging pressure was controlled in the terminal stages using a single step deformation to reduce the thickness of hot-pressed (SPS-ed isotropic) magnets. This low forging pressure at the terminal stage ( $750^\circ\text{C}$ ) prevents excessive cracking at the edges of the deformed magnet in rare-earth lean systems (like recycled HDDR nanocrystalline powder), rendering them useful for bulk applications after post-finishing and protective coating operations. Systematically, the effect of post-hot deformation thermal treatments on the magnetic properties was also established, which has not been investigated previously.

The development of textured recycled materials for the remanence enhancement is carried out in two steps: first, aligning the recycled powder in the applied magnetic field and then hot-pressing (SPS consolidation) to full density; secondly, hot-forging or deforming under higher pressures (100–150 MPa) with different dies and tooling to induce texture in the microstructure perpendicular to the pressing direction. Heating rate and pressure sequence during hot forging were optimized and the most suitable parameters are reported in this study. The pressure range was defined to factor the degree of deformation without compromising the coercivity, as the  $BH_{max}$  and remanence were enhanced by

low-pressure controlled hot forging. Taking pressure as a regulating factor helped us obtain texture in the bulk magnet, without exceptionally high strain rate or operating at very high forging temperatures. Therefore, the reported method can be adapted to sequentially tailor the magnetic properties of forged bulk magnets, which are better than the starting recycled HDDR Nd-Fe-B powder.

## 2. Contribution to the Field Statement

The bulk of the literature on the nanocrystalline Nd-Fe-B system has the vast majority of publications reporting melt-spun materials subjected to hot deformation. However, in this manuscript, we dealt only with the recycled HDDR Nd-Fe-B material. These two nanocrystalline Nd-Fe-B systems differ significantly and cannot be intermixed to devise results or a technological strategy. The progress of recycling with hydrogen-based technologies, like hydrogen decrepitation (HD) or hydrogenation–disproportionation–desorption–recombination (HDDR) processes is a widely applicable method for developing anisotropic and high coercivity bonded magnets with nanostructured  $\text{Nd}_2\text{Fe}_{14}\text{B}$  grains ( $\leq 400$  nm) and has drawn significant attention for the end-of-life scrap processing. The melt-spun ribbons as produced are never anisotropic and their grain size is less than 100 nm on average, such that hot-pressing results in exceptionally good magnetic properties. On the contrary, the remanence and maximum energy products are limited due to the isotropic nature of ribbons or pressed magnets. This makes a three-step process to develop anisotropy in melt-spun ribbons. Evidently, no method has ever been reported previously on the recycled HDDR Nd-Fe-B system to develop bulk anisotropic magnets.

The microstructure—i.e., nanocrystalline grain size, phase boundaries, and particle interface—is completely different in melt-spun ribbons and HDDR Nd-Fe-B and as a general comparison commercial, MQU-F grade melt-spun ribbons have  $H_{Ci} \approx 1560$  kA/m and  $B_r = 0.6$  T (isotropic flakes) while the commercial HDDR MF-15P powder has  $H_{Ci} \approx 1100$  kA/m and  $B_r = 1.35$  T (anisotropic powder). The mechanism of sintering, grain growth kinetics, grain morphology, grain boundary structure, and derivative magnetic properties thus are very different for the melt-spun ribbons and the HDDR Nd-Fe-B.

To the best of our knowledge, to date, there is not a single report on the hot deformation of the recycled HDDR Nd-Fe-B. Previously McGuinness et al. [9] and Li et al. [19] worked on the hot deformation of fresh HDDR Nd-Fe-B alloys, but their reported magnetic properties ( $BH_{max}$  and  $H_{Ci}$ ) are comparably inferior to our recycled material system. When we compare these reports to our previous publications, the remanence values are in the range of 0.7–0.8 T, returning  $M_r/M_S$  ratio  $\approx 0.5$  which indicates the isotropic nature of high coercivity magnets. After hot forging and 55% deformation ratio, we improved the remanence to 1.01 T which is  $\geq 23\%$  better than these isotropic magnets and subsequently  $M_r/M_S$  ratio improved to 0.64, indicating the production of anisotropic magnets. Additionally, the impact of thermal treatments on the microstructure and resultant magnetic properties has never been studied after the hot deformation of either commercial or recycled HDDR Nd-Fe-B system. This study validated these principles to devise industrial recycling and reprocessing strategy of rare-earth permanent magnets. Most importantly, we proposed a model to define the mechanism behind the improvement in the magnetic properties (simultaneously) after the thermal treatment. Hence, we believe these state-of-the-art values of remanence,  $BH_{max}$  and high coercivities warrant the recycled HDDR Nd-Fe-B system as a feasible method to recycle; and controlled hot forging can be expanded to the industrial scale for developing the texture in bulk magnets.

## 3. Materials and Methods

The recycled Nd-Fe-B powder was produced from the end-of-life (EOL) scrap magnets of composition:  $\text{Nd}_{13.4}\text{Dy}_{0.67}\text{Fe}_{78.6}\text{B}_{6.19}\text{Nb}_{0.43}\text{Al}_{0.72}$ , pulverized and reprocessed via the well-known dynamic hydrogenation–disproportionation–desorption–recombination (d-HDDR) method (controlled hydrogen pressure for anisotropy development in nanocrystalline  $\text{Nd}_2\text{Fe}_{14}\text{B}$  grains along c-axis by texture memory effect-TME) [36,37]. The oxygen content analysis was done with the Eltra ON 900 oxygen and nitrogen analyzer (Haan, Germany). Based on the density of elements and their



weight fractions in this composition, the theoretical density of the recycled powder was calculated as  $7.57 \pm 0.01 \text{ g/cm}^3$ . The magnetic properties of the recycled HDDR Nd-Fe-B powder were measured with the Lakeshore 7400 Series (Westerville, OH, USA) Vibrating Sample Magnetometer (VSM), capable of measurements up to 2 T applied fields.

The powder handling and sample preparation was done in controlled argon (Ar) atmosphere glove box with  $\text{O}_2$  content  $< 5 \text{ ppm}$  and  $\text{H}_2\text{O}$  content  $< 1 \text{ ppm}$ . About 3 g of the recycled HDDR Nd-Fe-B powder was poured into a 10 mm graphite dies with graphite spacers in between the solid punches at the top and bottom of the same material as the die. These powder containing dies were sealed in a vacuum bag within the glove box to avoid oxidation during further sample handling before sintering. Prior magnetic alignment with a 1.5 T applied field was carried out in the direction parallel to the pressing direction. The rapid sintering or hot-pressing operation was performed under dynamic vacuum of  $2 \times 10^{-2} \text{ mbar}$ , the graphite dies containing blends were put inside the Syntex 3000 (Fuji DR. SINTER, Saitama, Japan) SPS furnace. The sintering and hot forging pressure was regulated uniaxially with a pressure controller. The hot-pressing temperature was set to  $750^\circ\text{C}$  with a holding time of 1 min and the heating rate of  $700^\circ\text{C/min}$  with a final ramp of  $50^\circ\text{C/min}$  was maintained for the hot pressing. The temperature measurements were controlled by a calibrated infrared pyrometer. After the hot pressing, the samples were ground with SiC papers to remove the graphite spacers and the thickness of the cylindrical sample was reduced to 3 mm.

Hot deformation (hot forging) experiments were done also at  $700\text{--}800^\circ\text{C}$  for 1 min, with the 16 mm WC + Co sintered cermet dies under 200 mbar Ar (99.9% purity) atmosphere and the forging die pressure was varied from 100–150 MPa. A calibrated K-type thermocouple was inserted in the cermet die to control the hot forging processing temperatures to minimize overshooting to  $< 5^\circ\text{C}$  at peak conditions. The SPS operation was performed under  $2 \times 10^{-2} \text{ mbar}$  dynamic vacuum. A constant pressure of 40 MPa and relatively slow heating rate of  $50^\circ\text{C/min}$  was maintained up to the peak forging temperature in order to avoid high current density in the cermet dies, which otherwise may induce undesirable microstructural changes (grain growth, Nd-rich GB, and oxide phase transitions) [38]. Under these optimal settings, the heating rate was kept constant until the holding temperature in the range of  $700\text{--}800^\circ\text{C}$  was reached, but the pressure in the final  $50^\circ\text{C}$  step was subsequently increased to peak conditions of 100–150 MPa within one minute. A total of 3 min were given at the maximum pressure, i.e., one minute to reach the peak temperature, another one-minute holding at this hot-deformation temperature and the final one minute when the SPS current was switched off and cooling started instantly. The z-axis movement (up–down plunge of the SPS cermet dies) was recorded (as a measure against excessive cracking). The change in initial and final thickness was measured with the Vernier calipers to calculate the degree of deformation w.r.t forging pressure and temperatures.

The demagnetization measurements of bulk samples were taken on a permeameter (Magnet-Physik Dr. Steingroever, Cologne, Germany) after initially magnetizing along the c-axis. The relative density was determined with (Exelia AG DENSITEC, Zurich, Switzerland) bulk density-meter based on Archimedes principle by submerging the SPS processed samples in silicone oil.

After the hot deformation, the thermal treatment (annealing) was carried out at  $750^\circ\text{C}$  within the horizontal tube furnace (Carbolite Gero Limited, Hope Valley, UK) under  $> 10^{-5} \text{ mbar}$  vacuum and a heating rate of  $50^\circ\text{C/min}$ . The magnetic measurements were retaken after annealing. The samples were thermally demagnetized at  $450^\circ\text{C}$  for 10 min in the vacuum furnace ( $> 10^{-5} \text{ mbar}$ ). For the microscopic examination, the demagnetized samples were grinded by 2400 and 4000 grit size SiC papers. Final polishing was done with a  $1/4 \mu\text{m}$  diamond paste on the velvet cloth. The microstructural analysis was performed with JEOL 7600F, a Field Emission Scanning Electron Microscope (JEOL Ltd., Tokyo Japan) with an electron energy dispersive X-ray spectroscopy (EDXS) analysis fitted with a  $20 \text{ mm}^2$  Oxford X-Max detector (Oxford Instruments, High Wycombe, UK) for chemical and elemental identification, done at 20 keV.

#### 4. Results and Discussion

Summarized in Table 1, the starting EOL magnet had  $H_{Ci} = 1170$  kA/m and  $B_r = 1.19$  T which translated to the recycled HDDR powder having  $H_{Ci} = 830$  kA/m,  $J_r = 0.9$  T,  $J_S = 1.59$  T and  $BH_{max} = 124$  kJ/m<sup>3</sup> measured using a VSM with zero self-demagnetizing factor. The VSM measurements on the EOL scrap batches processed by HDDR method are shown in Figure 1, indicate the reprocessed batches are quite similar in polarization ( $J$ ) vs. applied field ( $H$ ) response, which indicates good consistency of results and recycling repeatability.

**Table 1.** Magnetic properties of the starting Nd-Fe-B materials prior to hot deformation.

Material Class	Coercivity $H_{Ci}$ (kA/m)	Remanence $B_r$ (T)	$BH_{max}$ (kJ/m <sup>3</sup> )	$M_r/M_S$ Ratio
End-of-Life (EOL) Scrap Magnet	1170	1.19	250	0.74
Recycled HDDR Powder	830	0.9	124	0.56
SPS Processed (Hot Pressed) Magnet	938	0.78	100	0.49
Post-SPS Annealed Magnets	1120–1160	0.79–0.8	100–110	0.5

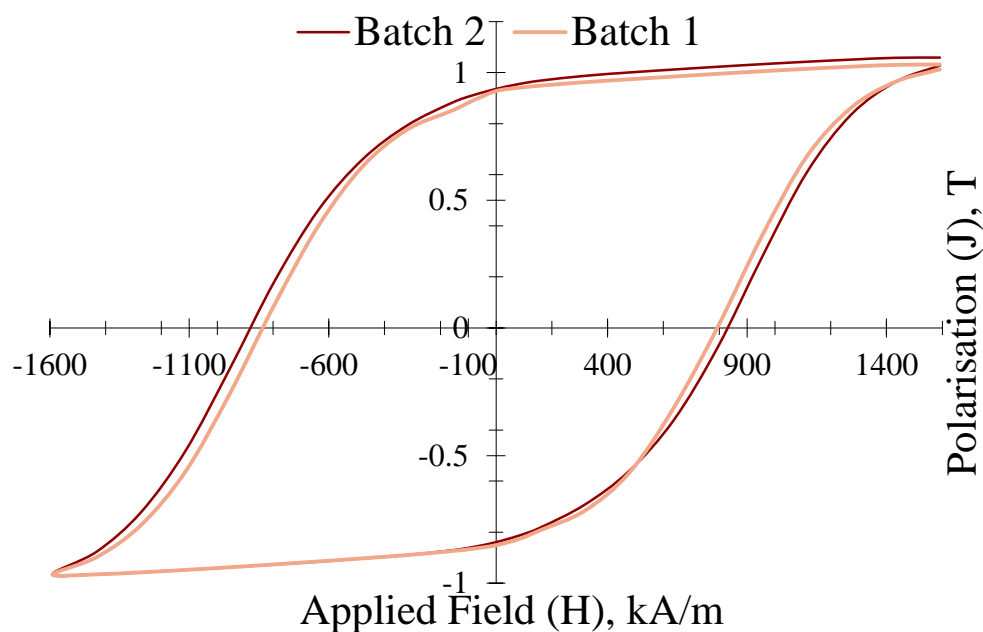


**Figure 1.** VSM analysis of recycled HDDR powder in two batches with approximately similar applied field vs. polarization response.

The oxygen content from the EOL magnet 2660 increased to 4760 ppm after the d-HDDR reprocessing in the recycled Nd-Fe-B powder [7]. Seemingly the oxygen content varies as the powder particle size is reduced below 100  $\mu\text{m}$  and it was found oxygen content nearly doubled for  $< 30$   $\mu\text{m}$  sized fractions. Therefore, the powder was not milled to prevent additional oxide phases which degrade sinterability, density, remanence (reduction in ferromagnetic phases) [8], and subsequently the texture from hot deformation [1,19]. The hot pressing conditions were kept similar to the previously reported SPS work [8] in order to achieve high coercivity and the optimal microstructure, i.e., at 750  $^{\circ}\text{C}$  for 1 min, 100 MPa uniaxial pressure and the post-SPS thermal treatment was also done for 1 h at 750  $^{\circ}\text{C}$  (above ternary transition temperature of 665  $^{\circ}\text{C}$ ) [7]. These annealed hot-pressed magnets had  $H_{Ci} \geq 1120$  kA/m and  $B_r \geq 0.79$  T, with  $M_r/M_S \approx 0.5$  indicating isotropic nature of the bulk magnets prior to hot deformation.

The average particle size of the recycled HDDR Nd-Fe-B powder (without any subsequent milling after d-HDDR) is 220  $\mu\text{m}$  and low magnification image can be seen for particles' morphology in Figure 2a. Each individually d-HDDR treated particles contains 240–400 nm sized  $\text{Nd}_2\text{Fe}_{14}\text{B}$  grains separated by thin Nd-rich phase (as in Figure 2b), which is discontinuous and non-uniformly distributed in the

microstructure of the recycled material as previously reported [7]. The effect of other elements in the composition of the HDDR powder (Dy, Nb, and Al) were also explained by Ikram et al. [7] to lower the eutectic transition temperature, such that Al is responsible for low temperature interactions (477 °C) with Nd/Dy at the Nd-rich grain boundary interface. The trace amount of Al in the composition stabilizes the  $\text{Nd}_2\text{Fe}_{14}\text{B}$  grain morphology and increasing the coercivity. The addition of Al in the HDDR powder has also been suggested to reduce the melting temperature of the RE-rich grain boundary phase [1,3]. The heavy rare-earth elements—such as Dy, Tb, Ho, etc.—are added as dopants to increase the coercivity and high temperature stability of the Nd-Fe-B magnets [2]. Whereas Nb is reported to form the  $\text{NbFe}_2$  Laves phase, which is finely dispersed in the nanocrystalline  $\text{Nd}_2\text{Fe}_{14}\text{B}$  matrix. The Laves phase does not contribute detrimentally to the magnetic properties of the HDDR Nd-Fe-B during SPS consolidation or hot pressing, as they scavenge the additional soft ferromagnetic  $\alpha$ -Fe during the recombination stage, which is necessary for retaining high coercivity in the HDDR system [7]. In a similar sense, the Laves phases are not anticipated to have deleterious effects during the hot deformation. The detailed phase analysis of the recycled HDDR powder is also presented in the preceding studies on explaining the oxygen content relationship to the particle size, microstructural changes, and sinterability [8].

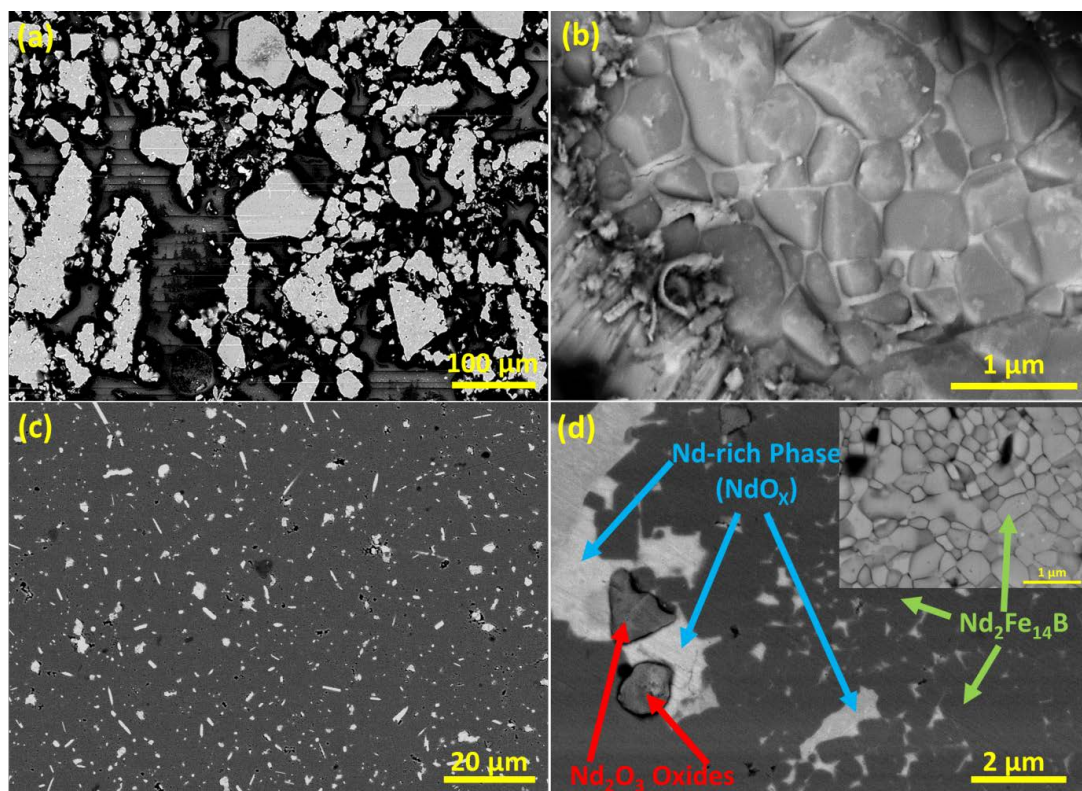


**Figure 2.** Backscattered electron (BSE) scanning electron microscope analysis of: (a) the recycled HDDR Nd-Fe-B powder particles of average 220 μm size and (b) fractal image at 20,000× magnification of approximately 400 nm sized  $\text{Nd}_2\text{Fe}_{14}\text{B}$  grains within each powder particle, (c) optimally hot pressed and fully dense recycled powder processed at 750 °C, (d) high magnification image of the hot pressed annealed sample showing constituent phases of different contrasts and inset showing submicron  $\text{Nd}_2\text{Fe}_{14}\text{B}$  grains exposed by etching with 3 M HCl and Cyphos ionic solution.

The microstructure of the 750 °C hot pressed sample is quite similar to the recycled HDDR powder (Figure 2c). It confirms that these conditions are suitable for attaining fully dense and high coercivity submicron sized  $\text{Nd}_2\text{Fe}_{14}\text{B}$  grains by restricting their exaggerated grain growth and avoiding unnecessary transformation of the Nd-rich phase to Nd-oxides at elevated temperatures, as observed in the inset of Figure 2d. The backscattered electron imaging (presented in Figure 2d) provides the contrast to identify different phases in the complex microstructure of HDDR Nd-Fe-B system with grey



matrix phase of submicron sized body centered tetragonal (bct)  $\text{Nd}_2\text{Fe}_{14}\text{B}$  grains,  $\text{Nd}_2\text{O}_3$  type oxides (cubic or hcp), and the bright intergranular Nd-rich phase (fcc-Nd or  $\text{NdO}_x$  type), which matches the previous reports [7,8]. The dark spots in the vicinity of matrix grains and triple pockets are pores.

The hot deformation at 100 MPa and temperature of 650 °C (below the ternary transition temperature of 665 °C [7], results not shown here) yielded  $H_{Ci} = 683$  kA/m and  $J_r = 0.64$  T ( $BH_{max} = 55$  kJ/m<sup>3</sup>) only. The remanence obtained in this case was significantly lower than the starting recycled powder. Therefore, in order to obtain better texturing in the hot-pressed samples, the temperature range was selected above this ternary transition temperature. Therefore, the hot deformation experiments were further performed at 100–150 MPa in the range of 700–800 °C. Further hot deformation temperatures higher than 800 °C, were not adapted in view of grain growth of the equiaxed and planar deformed grains which severely degrade the coercivity [14,19]. After hot deformation, these forged samples were subsequently annealed under vacuum at 750 °C for 1 h to recover the magnetic properties following strain relaxation and Nd-rich phase redistribution. Prolonging the hot forging to more than 1 min was found to have a detrimental effect on reprocessing of the HDDR Nd-Fe-B samples; therefore, further experiments were not evaluated beyond the optimized conditions.

For the hot deformation at 100 MPa pressure, the starting fully dense hot-pressed magnet after the thermal treatment had  $H_{Ci} \approx 1120$  kA/m,  $J_r = 0.8$  T and  $BH_{max} = 110$  kJ/m<sup>3</sup>. Figure 3 illustrates the polarization ( $J$ ) vs applied magnetic field ( $H$ ) results of hot deformed samples at working pressures of 100 and 150 MPa in the range of 700–800 °C, with the hold time of 1 min only. In the first case when the hot deformation pressure was 100 MPa, holding at 700 °C yielded  $J_r = 0.83$  T and  $H_{Ci} = 930$  kA/m, which indicates weak texturing for this applied pressure and low temperatures. The holding temperature of 750 °C resulted in  $J_r = 0.87$  T and  $H_{Ci} = 690$  kA/m after hot forging. The  $J_r$  increased to 0.89 T and  $H_{Ci}$  was 754 kA/m when deformed at 800 °C under 100 MPa pressure. A slightly higher temperature promotes annihilation of pores and nominal grain growth, which indicates that the optimally forged microstructure is developed in 800 °C, 100 MPa conditions (above the ternary transition temperature).

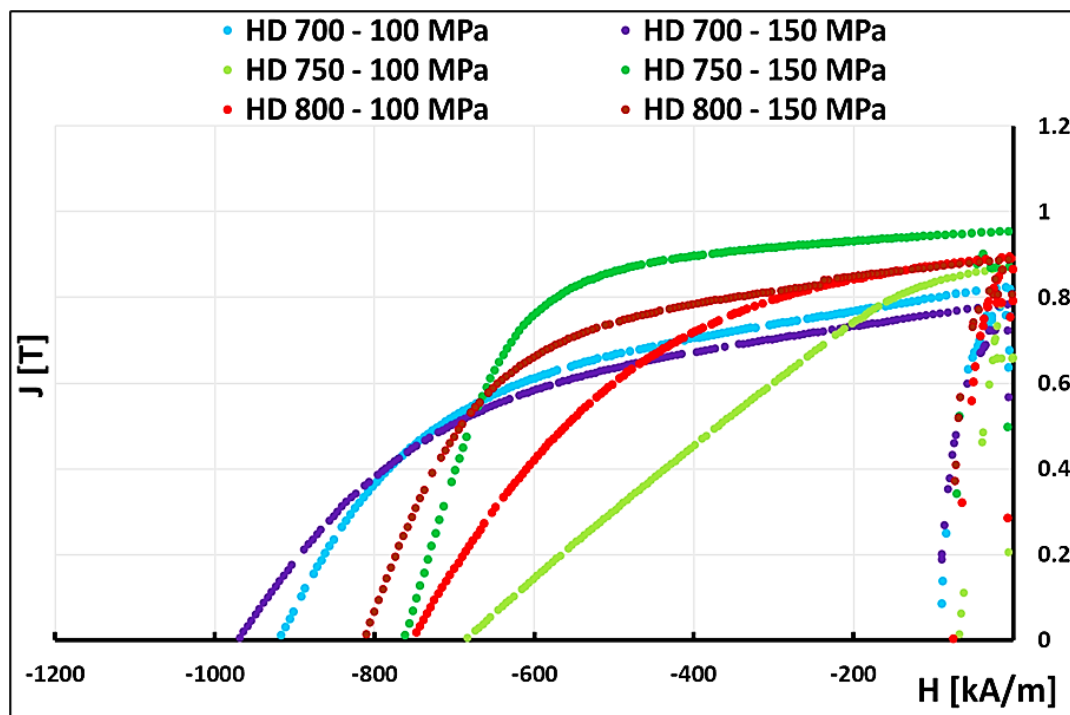


Figure 3. Comparison of the magnetic properties after hot deformation at 100 and 150 MPa.

At 700 °C, the onset of ternary transition is not complete yet, so the hot-forged samples retain the high coercivity of hot-pressed samples and the induced texture is very marginal in 100 and 150 MPa condition.

Comparing these findings with previous results on SPS processing, this slower ramp rate means low thermal stresses in the sample and  $H_{Ci}$  results are consistent with SPS reprocessing experiments [7].

As illustrated in Figure 3, by the application of higher hot deformation pressure at 150 MPa, the  $J_r$  increased in case of 750 °C sample to 0.96 T. On the contrary, at 800 °C, the remanence improvement over the 100 MPa forging was not observed with a similar value of  $J_r = 0.89$  T, possibly due to edging over the  $\text{Nd}_2\text{Fe}_{14}\text{B}$  grain growth regime at elevated temperature-pressure conditions [7,19,39]. The  $H_{Ci}$  in 150 MPa forging conditions followed a similar trend to 100 MPa samples, peaking at 990 kA/m at 700 °C to 767 kA/m at 750 °C and 817 kA/m at 800 °C. This improvement in the coercivity with temperature may be explained by the redistribution of the Nd-rich phase at the GBs and interfaces. The higher temperature and pressure conditions significantly reduce the porosity, so the Nd-rich phase achieves high wettability and transuses between the nanocrystalline grains via capillary action and compressing forces, resulting in coercivity improvement with the temperature at 150 MPa. The low forging pressure condition are appropriate to attain control in texturing and the degree of deformation, which resulted into better squareness of hysteresis loop and high coercivity. The controlled forging pressure was applied in a single step deformation in the terminal stage to reduce the thickness of hot-pressed (SPS-ed isotropic) magnets. This low pressure in the final bulk deformation stage (750 °C) prevented excessive cracking at the edges of the deformed magnet. Clearly, this approach is more suitable in rare-earth lean systems (e.g., recycled HDDR nanocrystalline powder).

The magnetic properties with post-hot deformation thermal treatment at 750 °C for 1 h in a comparative plot for all temperature regime (700–800 °C) is shown in Figure 4 and indicates the optimal results (in  $H_{Ci}$  and  $B_r$ , better than starting recycled powder) were obtained at 750 °C hot forging conditions. For the thermally treated samples forged at 100 MPa, the  $H_{Ci}$  improved for 750 and 800 °C which can be attributed to redistribution of intergranular phase and relaxation of deformation stresses. At 800 °C, 100 MPa, the range of improvement is lower than 750 °C, which can be explained with a possible grain growth in parallel and perpendicular directions as not enough room for redistribution may be available in the former case. For hot deformation at 700 °C, 100 MPa, the sample was characterized with surface cracking which may generate voids and dislocations under deformation. The hot-pressed sample had  $H_{Ci} > 1120$  kA/m which dropped to 930 kA/m after hot forging and slightly more to  $\approx 900$  kA/m with annealing. The slight decline in  $H_{Ci}$  after annealing can be attributed to inadequate redistribution of the Nd-rich phase below 746 °C (completion of ternary transition) into isolated voids that will not fully consolidate [7]. However, the remanence for all samples forged at 100 MPa pressure increased with the thermal treatments, as illustrated in Figure 4.

In the case of 150 MPa samples annealed at 750 °C, 1 h, the  $H_{Ci}$  increased subsequently for all the samples: 700 °C ( $H_{Ci} = 1007$  kA/m), 750 °C ( $H_{Ci} = 960$  kA/m), and very marginal for 800 °C sample ( $H_{Ci} = 820$  kA/m). This is due to the Nd-rich phase experiencing prominent wettability and high compressing forces during the forging stage at 800 °C, 150 MPa. Therefore, the liquid phase has already diffused (redistributed) along the grain boundary of the particles and between the nanocrystalline grains via pressure-assisted capillary action. Whereas, the 750 °C in both pressure ranges gained 200–350 kA/m coercivity improvement by thermal treatment because the Nd-rich phase was not uniformly redistributed during the slower ramp rate of 50 °C/min during the forging stage. The pressure assisted coalescence of microstructure at 50 °C/min effectively diffused the Nd-rich phase to the grain boundary regions, but at higher temperatures, it assists in grain growth [7]. The  $J_r$  of 150 MPa forging condition increased subsequently for the lower temperature samples, i.e., 700 °C (0.9 T) and 750 °C (1.01 T) after the thermal treatment. However, the remanence improvement was insignificant after the thermal treatment for 800 °C sample (0.89 → 0.9 T), which as previously explained is due to the completion of pressure-assisted coalescence and Nd-rich phase diffusion during forging at elevated temperatures [19]. This mild increment in  $J_r$  can be related to the relaxation of the processing stresses [7].

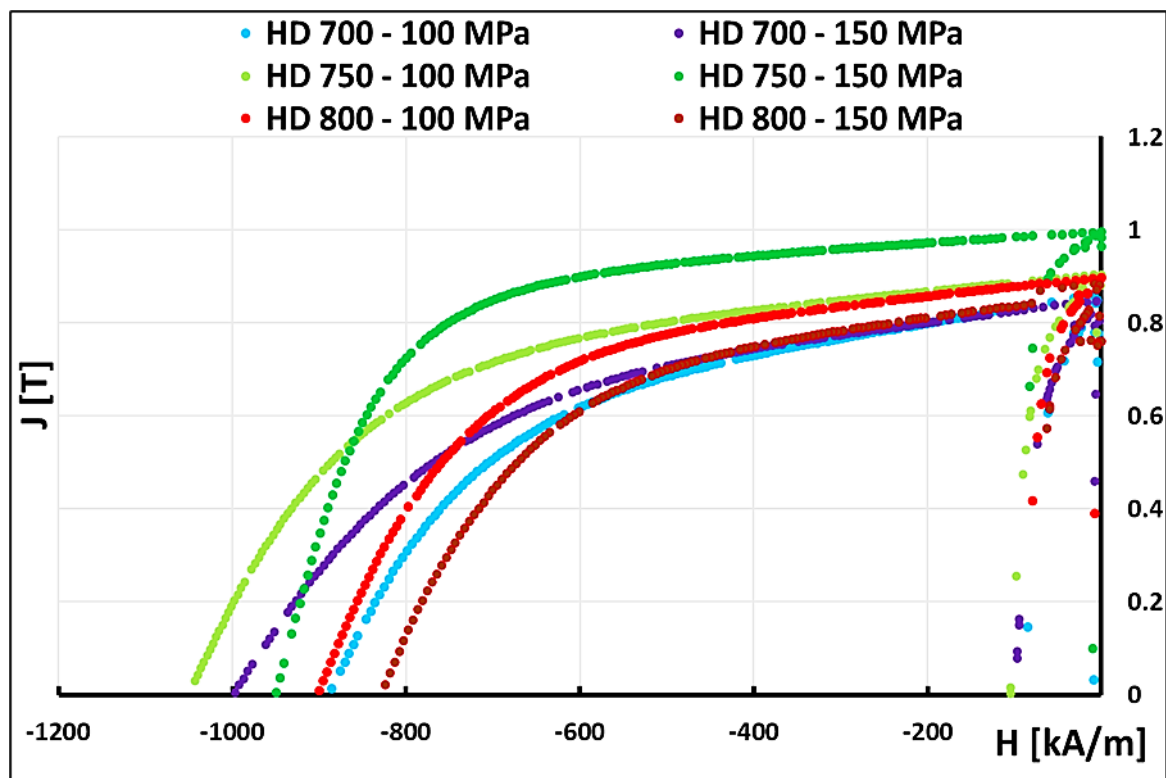


**Figure 4.** Comparative augmentation of magnetic properties of hot forged HDDR Nd-Fe-B magnets after vacuum post-processing thermal treatment at 750 °C for 1 h.

In short under low temperatures forging, the induced texture and  $J_r$  values are low, however the coercivity is high as the microstructure may correspond to hot-pressed magnets. As the temperature is increased at 100 MPa, texture development is better as  $J_r$  tends to increase and the annealing retains higher magnetic properties. With higher pressure—i.e., 150 MPa—the texture begins to develop at lower temperatures and the recovery of properties after the thermal treatment is mild since the hot deformation has already yielded the optimal microstructure. The thermal treatment for high temperature and pressure conditions correspond to stress relieving [7,8].

Moreover, under higher temperature–pressure conditions, the larger HDDR particles are prone to rupture and cracking, which could be associated with the 800 °C, 150 MPa sample not achieving high remanence as compared to 750 °C, 150 MPa [8]. These hot deformation-annealing results are in-line with the SPS study performed on the recycled HDDR Nd-Fe-B powders [8].

The 100 MPa hot-deformation process yielded  $\approx 40\%$  height reduction at 750 °C in the sample and the magnetic properties were:  $H_{Ci} = 690$  kA/m,  $J_r = 0.87$  T, and  $BH_{max} = 99$  kJ/m<sup>3</sup>. The hot deformation is a high strain process and therefore the stresses induced during the deformation can be considered to reduce the coercivity apart from the grain elongation [15,16,19,40]. The thermal treatment subsequently was performed at 750 °C for 1 h to release the microstructure of processing stresses and to also achieve the improvement in the magnetic properties due to the redistribution of the Nd-rich phase and the restructuring the surfaces of Nd<sub>2</sub>Fe<sub>14</sub>B matrix grain to accommodate the intergranular phase upon solidification [7]. Thus, after the heat treatment, the magnetic properties of 100 MPa hot forged sample improved to  $H_{Ci} \approx 1060$  kA/m,  $J_r = 0.91$  T, and  $BH_{max} = 144$  kJ/m<sup>3</sup>, as shown in Figure 5a and indicates a 12% improvement in remanence over the hot-pressed magnet at 0.79 T.

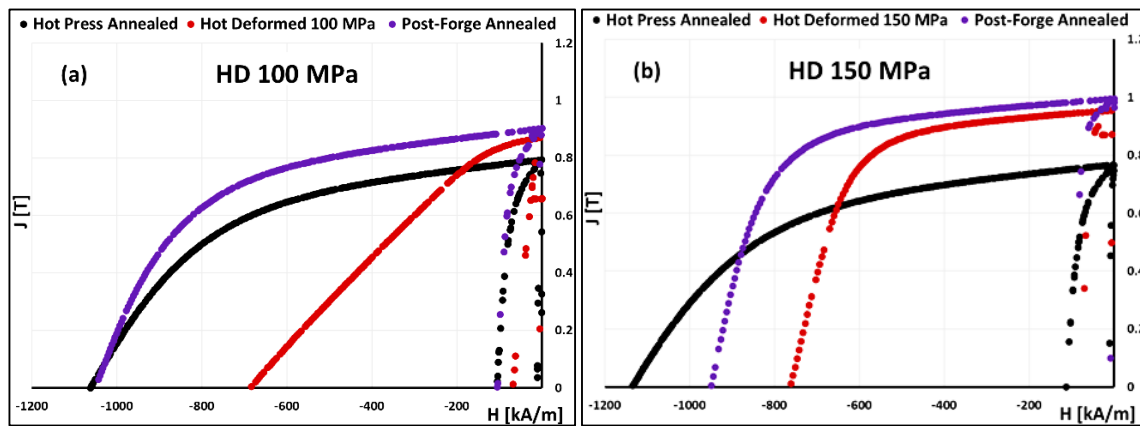


**Figure 5.** Comparison of the magnetic properties of recycled HDDR Nd-Fe-B based magnets optimally hot deformed at 750 °C under different forging pressures: (a) at 100 MPa and (b) 150 MPa. Plot legend: hot-pressing (black), hot-deformation (red), and post hot-deformation thermal treatment (purple).

Similarly, the hot-deformation experiments repeated at higher pressures resulted in better remanence than 100 MPa samples or hot-pressed magnets. The measured magnetic properties for the 750 °C, 150 MPa hot-deformed sample are illustrated in Figure 5b which gives  $\approx 23\%$  higher remanence with post-forging thermal treatment than isotropic hot-pressed magnets and 11% over the starting recycled anisotropic HDDR Nd-Fe-B powder. The heating rate was kept constant to 50 °C/min and during the final 3 min, the pressure was consequently maintained at 150 MPa in the second instance. The hot deformation pressure was increased rapidly from 40 MPa at 700 °C to 150 MPa at 750 °C within one minute to maximize the strain rate since a lower strain rate at high temperatures can cause grain coarsening as the deformation time is extended and the degree of alignment of the fine grains gets disturbed from the available Gibbs surface free (thermal) energy to undergo coarsening [14]. The magnetic properties of the starting hot-pressed magnet were:  $H_{Ci} \approx 1157$  kA/m,  $J_r = 0.79$  T, and  $BH_{max} = 103$  kJ/m<sup>3</sup>. The hot deformation at 150 MPa resulted in remanence enhancement and up to 55% height reduction. Therefore, the magnetic properties were measured to be:  $H_{Ci} \approx 770$  kA/m,  $J_r = 0.96$  T and  $BH_{max} = 165$  kJ/m<sup>3</sup>. Subsequently, the thermal treatment improved the overall magnetic properties and squareness of the loop in the hot-deformed magnet forged at 150 MPa, which were:  $H_{Ci} = 960$  kA/m,  $J_r = 1.01$  T, and  $BH_{max} = 180$  kJ/m<sup>3</sup>. In comparison, Li et al. [19] attained up to 69% height reduction with  $B_r = 1.22$  T and  $H_{Ci} = 181$  kA/m only from the fresh HDDR powder (possibly high degree of grain growth or hot forging stresses), measured parallel to the pressing direction.

In order to explain the behavior of remanence enhancement after annealing, we can systematically relate it according to the relationship of remanent magnetization [41]

$$M_r = A(1 - \beta) \frac{d}{d_0} \cos \theta M_S \quad (1)$$

In Equation (1),  $A$  denotes the positive parallel domains prior to the magnetic alignment,  $(1 - \beta)$  represents the volume fraction of hard magnetic phase ( $\text{Nd}_2\text{Fe}_{14}\text{B}$  in this case),  $d_0$  is theoretical density,  $d$  shows experimental density, the degree of orientation or texture is indicated by  $\cos \theta$  and  $M_S$  is the saturation magnetization. Therefore, a higher  $A$  factor indicates a low number of reverse magnetized domains in the system after annealing, as the  $H_{Ci}$  tends to increase as well due to microstructural factors (grain shape, morphology, stress relief, non-ferromagnetic grain boundary widening/decoupling effect, pinning field enhancement, and redistribution of Nd-rich phase). Moreover, no additional non-ferromagnetic additives were made part of hot-forging experiments, so  $A$  and  $\beta$  are not the influencing factors in hot deformation from Equation (1). Similarly, the densities of hot-forged and hot-pressed samples are nearly the same (99% of theoretical values, i.e., 7.57 g/cm<sup>3</sup>), so they are not affecting the remanence after thermal treatments either. The saturation magnetization ( $M_S$ ) remains largely unchanged before the HDDR reprocessing, hot pressing/deformation and subsequently annealing at 750 °C, 1 h. Therefore,



a 5% improvement in remanence from 0.96 to 1.01 T is invariably linked to the degree of texturing perpendicular to the pressing direction which tends to get reduced subsequently after the thermal treatment. The microstructure composed of highly textured  $\text{Nd}_2\text{Fe}_{14}\text{B}$  grains is beneficial for preferential grain growth during hot deformation and which will impart favorable remanence enhancement. In the case of nanocrystalline melt-spun ribbons, Wang et al. [41] identified with EBSD that the texture in platelet shaped layers on the basal plane was enhanced by increasing the annealing time. Moreover, the oriented platelet grains, although followed inhomogeneous grain growth pattern but suppressed the abnormal grain growth of non-aligned coarse grains and the number of mis-oriented grains decreased after annealing. Although EBSD was out of the scope of this research but the model from Equation (1) advocate the degree of orientation  $\cos \theta$  of  $\text{Nd}_2\text{Fe}_{14}\text{B}$  hard phase grain tends to increase after the thermal treatment due to grain surface restructuring (both aligned and coarse non-aligned grains), besides relaxation of the forging stresses is also a contributing factor. Since the thermal treatments were performed above the ternary transition temperature of 665 °C, it may also be expected that the intergranular phases experience non-ferromagnetic transformations, which effectively improves the localized exchange decoupling behavior [41–44], however, such a study has not been proven on the HDDR Nd-Fe-B system.

In Nd-lean HDDR powder (e.g., recycled), the stress induced crystallographic orientation of the nanocrystalline grains by hot deformation is difficult and can only be achieved by critically controlling the forging parameters coupled with stress-relief thermal treatments. The applicable pressure of 150 MPa was in a sense limit for the operation mode and a further increase was not possible on this system. Therefore, from the comparison of 100 and 150 MPa range, the improvement (10%) is evident at 0.1 T approximately for 50 MPa increase. Thereby, if the system allowed hot deformation up to 500 MPa, the recycled HDDR powder is capable of reaching the remanence values much higher than these obtained but at a severe toll on coercivity as previous studies have shown for height reductions greater than 50% [17,45,46].

The cross sections of hot deformed magnets prepared at 750 °C were characterized for their microstructure by HR-SEM in backscattered electron imaging mode as shown in Figure 6. The pressing direction in each case is indicated by the arrows. As clearly seen from Figure 6a, when the hot deformation pressure is low at 100 MPa only, the microstructure is similar to the initial recycled HDDR Nd-Fe-B powder or the hot-pressed (optimally SPS-ed) samples in Figure 2. The equiaxed and the platelet-shaped grains both coexist with a poor degree of alignment due to inadequate deformation as marked with the red arrows in Figure 6a. Apart from only a few grains, the majority of the  $\text{Nd}_2\text{Fe}_{14}\text{B}$  grains are not aligned after hot deformation with the pressing direction, as represented in Figure 6b. This suggests incomplete hot-deformation or the lack of uniform texture in the sample. The matrix grains are also not excessively deformed (Figure 6b), which is the reason for higher coercivity than the starting material. After the thermal treatment, we can expect the relaxation of deformation stresses, which improved the overall magnetic properties.

In the case of hot deformation at 150 MPa pressure, the microstructure in Figure 6c is more appropriately textured and several grains are deformed perpendicular to the pressing direction which resulted in higher  $B_r$ . In this case, the two-zone microstructure is not distinguishable as clearly the grains are suitably deformed when magnified in Figure 6d with the pressing direction. At 750 °C forging temperature, overall limited grain growth in equiaxed manner or perpendicular to the pressing direction was observed which is suitable to conserve the magnetic properties of the starting recycled powder. Higher forging pressure resulted in a larger degree of deformation and thereby improvement in the texture is apparent. The very high degree of deformation (above 80%) results in nanocrystalline grains elongated beyond  $> 1 \mu\text{m}$  size [14,15]. The elongation of matrix grains is also considered as grain growth and consequently, the demagnetizing field will be higher on severely deformed grain surfaces, so the coercivity starts to decrease as grains begin to grow, but more importantly with higher percentage reduction in height, the deformation stresses on the microstructure are higher, which degrade the  $H_{Ci}$  [15,16,19,40]. The in-homogeneities in the crystal structure, as well as the surface imperfections generated after hot deformation, are apparently the local sites for initiating demagnetization. The defects

like irregularly shaped grains, non-ferromagnetic inclusions/grain boundaries, surface or geometric defects, etc. become the sites for local nucleation fields  $H_N$  (regions favoring magnetization reversal). These defects reduce the coercivity to

$$H_{Ci} = \alpha H_a - N_{\text{eff}} M_S \quad (2)$$

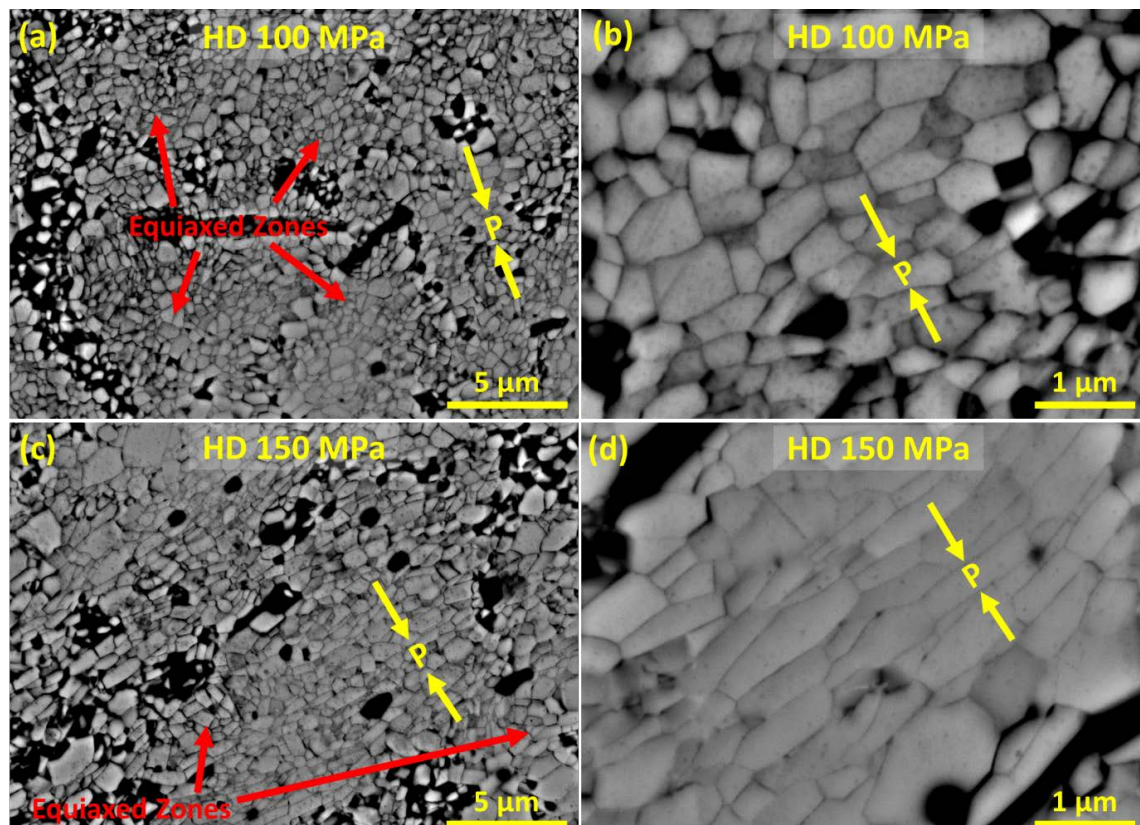


**Figure 6.** BSE micrographs of (non-annealed) hot deformed samples at (a) 100 MPa with two zone microstructure, (b) 100 MPa at high magnification indicating the pressing direction, and (c) 150 MPa with minimal equiaxed grains; and (d) 20,000× magnification of hot deformed  $\text{Nd}_2\text{Fe}_{14}\text{B}$  grains; the arrows indicate the direction of pressing with “P” during SPS hot deformation.

Here in Equation (2),  $H_a$  is the anisotropy field, the Kronmüller’s factor  $\alpha \approx 0.2\text{--}0.5$  and the effective demagnetizing factor ( $N_{\text{eff}} \approx 0.8\text{--}1.7$  [10]). The deformed platelet-shaped grains largely increase the  $N_{\text{eff}}$  value and the possible accelerated grain growth above 800 °C is reasoned to degrade the coercivity [14]. During the hot deformation, it has been advocated that the liquid grain boundary phase is squeezed out above the ternary transition temperature of 665 °C as it rotates and gets redistributed along with the smaller aspect ratio grain facets [47]. Therefore, the Nd-rich phase perpendicular to the pressing direction is forced out of the intergranular regions where textured parallel facing grains get into intermittent contact with each other. Therefore, the localized exchange coupling effects at these regions without the Nd-rich phase contribute to the lowering of the coercivity [17]. With the release of interfacial energy from the liquid Nd-rich phase during hot deformation, the stress concentration gets developed in the contact points and triple pockets which can lead to the formation of non-aligned grains in the vicinity thereby necessitates the annealing treatment [14]. In regions where the grain boundaries are absent, the nanocrystalline  $\text{Nd}_2\text{Fe}_{14}\text{B}$  grains can rapidly grow above the ternary transition temperature and the lattice mismatch is gradually truncated, which will also release lattice from distortion under reprocessing (thermally induced) stresses [41]. This study verified that potential is very high for the HDDR Nd-Fe-B based commercial as well as recycled materials and provides the

fundamental understanding of hot deformation application on the recycled HDDR Nd-Fe-B alloys, defining the limits for coercivity, processing conditions, annealing, and controlled texture development.

Henceforth, with the application of higher deformation pressures and the subsequent addition of low melting eutectic alloys or RE-rich nanoparticles blends, not only the remanence enhancement and  $BH_{max}$  are possible but coercivity can also be improved in low grade recycled materials. This scope of simultaneous improvement of  $H_{Ci}$  after hot deformation on the recycled HDDR Nd-Fe-B is currently under investigation and further results shall be explained in an alternate report.

## 5. Conclusions

This short study determines that the SPS hot pressed recycled HDDR Nd-Fe-B powder has coercivity values slightly higher than the commercial HDDR MF-15P powder because of the initial HDDR grain-size, microstructure preservation, and the SPS processing control. The achieved magnetic properties imply that the recycled HDDR Nd-Fe-B system can still achieve an optimal level of magnetic properties after hot deformation and without the addition of excessive Nd content, by controlling the forging parameters and supplementary thermal treatments. The application of higher pressures during hot deformation can develop texture in these originally isotropic magnets. The hot deformation pressure of 150 MPa resulted in 55% reduction in height and improvement in  $J_r$  to 0.96 T which is subsequently improved to 1.01 T ( $BH_{max} = 180 \text{ kJ/m}^3$ ) after the thermal treatment at 750 °C for 1 h, i.e.,  $\approx 11\%$  improvement over the recycled magnetic powder. This reduced pressure optimal hot deformation suitably retains high coercivity and imparts texture, which evidentially yields magnetic properties better than the starting recycled HDDR Nd-Fe-B powder.

**Author Contributions:** Conceptualization, A.I.; Methodology, A.I.; Software, A.I.; Validation, A.I. and M.A.; Formal analysis, A.I.; Investigation, A.I.; Resources, M.A., R.S. and A.W.; Data curation, A.I.; Writing—original draft preparation, A.I.; Writing—review and editing, A.I., M.A. and F.P.; Visualization, A.I.; Supervision, S.K., A.W., K.Ž.R. and F.P.; Project administration, K.Ž.R., S.K. and A.W.; Funding acquisition, S.K., A.W. and K.Ž.R. All authors have read and agreed to the published version of the manuscript.

**Funding:** The study leading to these results has received the funding from the European Community's Horizon 2020 Program ([H2020/2014-2019]) under grant agreement no. 674973 (MSCA-ETN DEMETER). Project website: <http://etn-demeter.eu/>. This publication reflects only the authors' research findings, which are targeted to contribute to the betterment of the global community

**Acknowledgments:** The authors aptly acknowledge the Department for Nanostructured Materials (K7 Nano) for provisioning the magnet synthesis/measurement facilities and the Center for Electron Microscopy & Microanalysis (CEMM) for scanning electron microscopy support at the Jožef Stefan Institute, Slovenia.

**Conflicts of Interest:** The authors declare no conflict of interest.

## References

1. Sugimoto, S. Current status and recent topics of rare-earth permanent magnets. *J. Phys. D Appl. Phys.* **2011**, *44*, 6. [CrossRef]
2. Gutfleisch, O. Controlling the properties of high energy density permanent magnetic materials by different processing routes. *J. Phys. D Appl. Phys.* **2000**, *33*, 16. [CrossRef]
3. Morimoto, K.; Katayama, N.; Akamine, H.; Itakura, M. Coercivity enhancement of anisotropic Dy-free Nd-Fe-B powders by conventional HDDR process. *J. Magn. Magn. Mater.* **2012**, *324*, 3723–3726. [CrossRef]
4. Coey, J.M.D. *Magnetism and Magnetic Materials*; Cambridge University Press: New York, NY, USA, 2010.
5. Kimiabeigi, M.; Sheridan, R.S.; Widmer, J.D.; Walton, A.; Farr, M.; Scholes, B.; Harris, I.R. Production and Application of HPMS Recycled Bonded Permanent Magnets for a Traction Motor Application. *IEEE Trans. Ind. Electron.* **2018**, *65*, 3795–3804. [CrossRef]
6. Nakamura, H. The current and future status of rare earth permanent magnets. *Scr. Mater.* **2018**, *154*, 273–276. [CrossRef]

7. Ikram, A.; Mehmood, M.F.; Podlogar, M.; Eldosouky, A.; Sheridan, R.S.; Awais, M.; Walton, A.; Kržmanc, M.M.; Tomše, T.; Kobe, S.; et al. The sintering mechanism of fully dense and highly coercive Nd-Fe-B magnets from the recycled HDDR powders reprocessed by spark plasma sintering. *J. Alloys Compd.* **2019**, *774*, 1195–1206. [[CrossRef](#)]
8. Ikram, A.; Mehmood, F.; Sheridan, R.S.; Awais, M.; Walton, A.; Eldosouky, A.; Šturm, S.; Kobe, S.; Rožman, K.Ž. Particle size dependent sinterability and magnetic properties of recycled HDDR Nd-Fe-B powders consolidated with spark plasma sintering. *J. Rare Earths* **2020**, *38*, 90–99. [[CrossRef](#)]
9. McGuinness, P.J.; Short, C.; Wilson, A.F.; Harris, I.R. The production and characterization of bonded, hot-pressed and die-upset HDDR magnets. *J. Alloys Compd.* **1992**, *184*, 243–255. [[CrossRef](#)]
10. Cullity, B.D.; Graham, C.D. *Introduction to Magnetic Materials*, 2nd ed.; IEEE/Wiley: Hoboken, NJ, USA, 2009.
11. Güth, K.; Woodcock, T.G.; Thielsch, J.; Schultz, L.; Gutfleisch, O. Local orientation analysis by electron backscatter diffraction in highly textured sintered, die-upset, and hydrogenation disproportionation desorption and recombination Nd-Fe-B magnets. *J. Appl. Phys.* **2011**, *109*, 07A764. [[CrossRef](#)]
12. Sepehri-Amin, H.; Ohkubo, T.; Hono, K.; Güth, K.; Gutfleisch, O. Anisotropy inducement mechanism in hydrogen disproportionation (HDDR) processed Nd-Fe-B powders. *J. Magn. Soc. Jpn.* **2014**, *38*, 37–44.
13. Kim, T.-H.; Oh, J.-S.; Cha, H.-R.; Lee, J.-G.; Kwon, H.-W.; Yang, C.-W. Direct observation of texture memory in hydrogenation–disproportionation–desorption–recombination processed Nd-Fe-B magnets using electron backscatter diffraction. *Scr. Mater.* **2016**, *115*, 6–9. [[CrossRef](#)]
14. Chen, R.J.; Wang, Z.X.; Tang, X.; Yin, W.Z.; Jin, C.X.; Ju, J.Y.; Lee, D.; Yan, A.R. Rare earth permanent magnets prepared by hot deformation process. *Chin. Phys. B* **2018**, *27*, 117504. [[CrossRef](#)]
15. Müller, K.H.; Grünberger, W.; Hinz, D.; Gebel, B.; Eckert, D.; Handstein, A. Hot deformed HDDR Nd-Fe-B permanent magnets. *Mater. Lett.* **1998**, *34*, 50–54. [[CrossRef](#)]
16. Liesert, S.; Kirchner, A.; Grünberger, W.; Handstein, A.; de Rango, P.; Fruchart, D.; Schultz, L.; Müller, K.H. Preparation of anisotropic NdFeB magnets with different Nd contents by hot deformation (die-upsetting) using hot-pressed HDDR powders. *J. Alloys Compd.* **1998**, *266*, 260–265. [[CrossRef](#)]
17. Gopalan, R.; Sepehri-Amin, H.; Suresh, K.; Ohkubo, T.; Hono, K.; Nishiuchi, T.; Nozawa, N.; Hirosawa, S. Anisotropic Nd-Fe-B nanocrystalline magnets processed by spark plasma sintering and in situ hot pressing of hydrogenation–decomposition–desorption–recombination powder. *Scr. Mater.* **2009**, *61*, 978–981. [[CrossRef](#)]
18. Li, X.; Chen, Z.; Yang, C.; Qu, S. NdFeB Magnets Prepared by Spark Plasma Sintering and Hot Deformation, Xiyu Jinshu Cailiao Yu Gongcheng/Rare. *Met. Mater. Eng.* **2013**, *42*, 194–199.
19. Li, X.-Q.; Li, L.; Hu, K.; Chen, Z.-C.; Qu, S.-G.; Yang, C. Microstructure and magnetic properties of anisotropic Nd-Fe-B magnets prepared by spark plasma sintering and hot deformation. *Trans. Nonferrous Met. Soc. China* **2014**, *24*, 3142–3151. [[CrossRef](#)]
20. Xu, X.D.; Sepehri-Amin, H.; Sasaki, T.T.; Soderžnik, M.; Tang, X.; Ohkubo, T.; Hono, K. Comparison of coercivity and squareness in hot-deformed and sintered magnets produced from a Nd-Fe-B-Cu-Ga alloy. *Scr. Mater.* **2019**, *160*, 9–14. [[CrossRef](#)]
21. Song, J.; Guo, S.; Ding, G.F.; Chen, K.; Chen, R.J.; Lee, D.; Yan, A. Boundary structure modification and coercivity enhancement of the Nd-Fe-B magnets with TbCu doping by the process of pre-sintering and hot-pressing. *J. Magn. Magn. Mater.* **2019**, *469*, 613–617. [[CrossRef](#)]
22. Soderžnik, M.; Li, J.; Liu, L.H.; Sepehri-Amin, H.; Ohkubo, T.; Sakuma, N.; Shoji, T.; Kato, A.; Schrefl, T.; Hono, K. Magnetization reversal process of anisotropic hot-deformed magnets observed by magneto-optical Kerr effect microscopy. *J. Alloys Compd.* **2019**, *771*, 51–59. [[CrossRef](#)]
23. Li, J.; Liu, L.H.; Sepehri-Amin, H.; Tang, X.; Ohkubo, T.; Sakuma, N.; Shoji, T.; Kato, A.; Schrefl, T.; Hono, K. Coercivity and its thermal stability of Nd-Fe-B hot-deformed magnets enhanced by the eutectic grain boundary diffusion process. *Acta Mater.* **2018**, *161*, 171–181. [[CrossRef](#)]
24. Castle, E.; Sheridan, R.; Zhou, W.; Grasso, S.; Walton, A.; Reece, M.J. High coercivity, anisotropic, heavy rare earth-free Nd-Fe-B by Flash Spark Plasma Sintering. *Sci. Rep.* **2017**, *7*, 11134. [[CrossRef](#)] [[PubMed](#)]
25. Kim, T.-H.; Lee, S.-R.; Yun, S.J.; Lim, S.H.; Kim, H.-J.; Lee, M.-W.; Jang, T.-S. Anisotropic diffusion mechanism in grain boundary diffusion processed Nd-Fe-B sintered magnet. *Acta Mater.* **2016**, *112*, 59–66. [[CrossRef](#)]
26. Castle, E.; Sheridan, R.; Grasso, S.; Walton, A.; Reece, M. Rapid sintering of anisotropic, nanograined Nd-Fe-B by flash-spark plasma sintering. *J. Magn. Magn. Mater.* **2016**, *417*, 279–283. [[CrossRef](#)]



27. Sepehri-Amin, H.; Liu, L.H.; Ohkubo, T.; Yano, M.; Shoji, T.; Kato, A.; Schrefl, T.; Hono, K. Microstructure and temperature dependent of coercivity of hot-deformed Nd-Fe-B magnets diffusion processed with Pr-Cu alloy. *Acta Mater.* **2015**, *99*, 297–306. [\[CrossRef\]](#)
28. Liu, J.; Sepehri-Amin, H.; Ohkubo, T.; Hioki, K.; Hattori, A.; Schrefl, T.; Hono, K. Grain size dependence of coercivity of hot-deformed Nd-Fe-B anisotropic magnets. *Acta Mater.* **2015**, *82*, 336–343. [\[CrossRef\]](#)
29. Sepehri-Amin, H.; Liu, J.; Ohkubo, T.; Hioki, K.; Hattori, A.; Hono, K. Enhancement of coercivity of hot-deformed Nd-Fe-B anisotropic magnet by low-temperature grain boundary diffusion of Nd<sub>60</sub>Dy<sub>20</sub>Cu<sub>20</sub> eutectic alloy. *Scr. Mater.* **2013**, *69*, 647–650. [\[CrossRef\]](#)
30. Liu, L.H.; Sepehri-Amin, H.; Ohkubo, T.; Yano, M.; Kato, A.; Sakuma, N.; Shoji, T.; Hono, K. Coercivity enhancement of hot-deformed Nd-Fe-B magnets by the eutectic grain boundary diffusion process using Nd<sub>62</sub>Dy<sub>20</sub>Al<sub>18</sub> alloy. *Scr. Mater.* **2017**, *129*, 44–47. [\[CrossRef\]](#)
31. Seelam, U.M.R.; Liu, L.H.; Akiya, T.; Sepehri-Amin, H.; Ohkubo, T.; Sakuma, N.; Yano, M.; Kato, A.; Hono, K. Coercivity of the Nd-Fe-B hot-deformed magnets diffusion-processed with low melting temperature glass forming alloys. *J. Magn. Magn. Mater.* **2016**, *412*, 234–242. [\[CrossRef\]](#)
32. Akiya, T.; Liu, J.; Sepehri-Amin, H.; Ohkubo, T.; Hioki, K.; Hattori, A.; Hono, K. High-coercivity hot-deformed Nd-Fe-B permanent magnets processed by Nd-Cu eutectic diffusion under expansion constraint. *Scr. Mater.* **2014**, *81*, 48–51. [\[CrossRef\]](#)
33. Song, T.; Tang, X.; Yin, W.; Chen, R.; Yan, A. Coercivity enhancement of hot-pressed magnet prepared by HDDR Nd-Fe-B powders using Pr-Cu eutectic alloys diffusion. *J. Magn. Magn. Mater.* **2019**, *471*, 105–109. [\[CrossRef\]](#)
34. Wang, H.H.; Chen, R.J.; Yin, W.Z.; Zhu, M.Y.; Tang, X.; Wang, Z.X.; Jin, C.X.; Ju, J.Y.; Lee, D.; Yan, A. The effect of Nd-Cu diffusion during hot pressing and hot deformation on the coercivity and the deformation ability of Nd-Fe-B HDDR magnets. *J. Magn. Magn. Mater.* **2017**, *438*, 35–40. [\[CrossRef\]](#)
35. Cha, H.R.; Jeon, K.W.; Yu, J.H.; Kwon, H.W.; Kim, Y.D.; Lee, J.G. Coercivity enhancement of hot-deformed Nd-Fe-B magnet by grain boundary diffusion process using the reaction of NdHX and Cu nanopowders. *J. Alloys Compd.* **2017**, *693*, 744–748. [\[CrossRef\]](#)
36. Sheridan, R.S.; Sillitoe, R.; Zakotnik, M.; Harris, I.R.; Williams, A. Anisotropic powder from sintered NdFeB magnets by the HDDR processing route. *J. Magn. Magn. Mater.* **2012**, *324*, 63–67. [\[CrossRef\]](#)
37. Sheridan, R.S.; Williams, A.J.; Harris, I.R.; Walton, A. Improved HDDR processing route for production of anisotropic powder from sintered NdFeB type magnets. *J. Magn. Magn. Mater.* **2014**, *350*, 114–118. [\[CrossRef\]](#)
38. Ikram, A.; Mehmood, M.F.; Samardzija, Z.; Sheridan, R.S.; Awais, M.; Walton, A.; Šturm, S.; Kobe, S.; Žužek, R.K. Coercivity Increase of the Recycled HDDR Nd-Fe-B Powders Doped with DyF<sub>3</sub> and Processed via Spark Plasma Sintering & the Effect of Thermal Treatments. *Materials (Basel)* **2019**, *12*, 1498.
39. Seelam, U.M.R.; Ohkubo, T.; Abe, T.; Hirose, S.; Hono, K. Faceted shell structure in grain boundary diffusion-processed sintered Nd-Fe-B magnets. *J. Alloys Compd.* **2014**, *617*, 884–892. [\[CrossRef\]](#)
40. Kirchner, A.; Grünberger, W.; Gutfleisch, O.; Neu, V.; Müller, K.H.; Schultz, L. A comparison of the magnetic properties and deformation behaviour of Nd-Fe-B magnets made from melt-spun, mechanically alloyed and HDDR powders. *J. Phys. D Appl. Phys.* **1998**, *31*, 1660–1666. [\[CrossRef\]](#)
41. Wang, Z.; Ju, J.; Wang, J.; Yin, W.; Chen, R.; Li, M.; Jin, C.; Tang, X.; Lee, D.; Yan, A. Magnetic Properties Improvement of Die-upset Nd-Fe-B Magnets by Dy-Cu Press Injection and Subsequent Heat Treatment. *Sci. Rep.* **2016**, *6*, 38335. [\[CrossRef\]](#)
42. Hono, K.; Sepehri-Amin, H. Strategy for high-coercivity Nd-Fe-B magnets. *Scr. Mater.* **2012**, *67*, 530–535. [\[CrossRef\]](#)
43. Kim, T.-H.; Lee, S.-R.; Lee, M.-W.; Jang, T.-S.; Kim, J.W.; Kim, Y.D.; Kim, H.-J. Dependence of magnetic, phase-transformation and microstructural characteristics on the Cu content of Nd-Fe-B sintered magnet. *Acta Mater.* **2014**, *66*, 12–21. [\[CrossRef\]](#)
44. Mouri, T.; Kumano, M.; Yasuda, H.Y.; Nagase, T.; Kato, R.; Nakazawa, Y.; Shimizu, H. Effect of two-stage deformation on magnetic properties of hot-deformed Nd-Fe-B permanent magnets. *Scr. Mater.* **2014**, *78–79*, 37–40. [\[CrossRef\]](#)
45. Sadullahoğlu, G.; Altunçevahir, B.; Okan, A.A. Investigation of Grain Boundary Compositions and Magnetic Properties of Hot-Worked Nd<sub>18</sub>Tb<sub>1</sub>Fe<sub>66.5</sub>Co<sub>5</sub>Al<sub>1.5</sub>B<sub>8</sub> Magnets. *Acta Phys. Pol. A* **2013**, *123*, 233–234. [\[CrossRef\]](#)

46. Liu, Z.W.; Huang, Y.L.; Hu, S.L.; Zhong, X.C.; Yu, H.Y.; Gao, X.X. Properties enhancement and recoil loop characteristics for hot deformed nanocrystalline NdFeB permanent magnets. *IOP Conf. Ser. Mater. Sci. Eng.* **2014**, *60*, 012013. [[CrossRef](#)]
47. Bance, S.; Seebacher, B.; Schrefl, T.; Exl, L.; Winklhofer, M.; Hrkac, G.; Zimanyi, G.; Shoji, T.; Yano, M.; Sakuma, N.; et al. Grain-size dependent demagnetizing factors in permanent magnets. *J. Appl. Phys.* **2014**, *116*, 233903. [[CrossRef](#)]



© 2020 by the authors. Licensee MDPI, Basel, Switzerland. This article is an open access article distributed under the terms and conditions of the Creative Commons Attribution (CC BY) license (<http://creativecommons.org/licenses/by/4.0/>).